DOI: 10.13009/EUCASS2017-86

Dynamic layer formation in the reattachment zone for a supersonic laminar separated flow

Valeriy I. Zapryagaev, Ivan N. Kavun*, Lukeriya .P. Trubitsyna**

**Khristianovich Institute of Theoretical and Applied Mechanics, Siberian Branch, Russian Academy of Sciences, 630090, Novosibirsk, Russia*

Abstract

Results of an experimental study of the flow structure in the region of reattachment of a supersonic laminar separated flow are reported. The separated flow is generated by a model shaped as a compression corner consisting of a horizontal flat plate followed by a ramp. The model with is equal to the plate length from the leading edge to the plate/ramp junction line. The ramp angle is varied in the interval $\varphi = 20° – 50°$. The free-stream Mach number is $M_\infty = 6$ or 8. The analysis of the Pitot pressure profiles near the ramp wall in the downstream direction behind the reattachment line confirms the existence of a high-pressure layer with the total pressure being appreciably greater than in the surrounding flow.

Nomenclature

l – streamwise coordinate (directed downstream along the model),
L – length of the horizontal flat plate,
M – Mach number,
M_m – mean Mach number in the considered domain,
M_{Sd} – standard deviation of the Mach number from the mean value M_m,
M_∞ – free-stream Mach number,
p – pressure,
p_0 – total pressure,
$p_{0\infty}$ – free-stream total pressure,
p_{Pt} – Pitot pressure measured by the probe,
p_w – near-wall pressure (pressure on the model surface),
r – normal coordinate (perpendicular to the model surface),
R – radius of curvature of the leading edge of the flat plate,
Re – Reynolds number,
Re_L – Reynolds number based on the plate length L,
T – temperature,
T_0 – total temperature,
$T_{0\infty}$ – free-stream total temperature,
x – horizontal coordinate in the free-stream direction,
y – vertical coordinate,
z – transverse coordinate (forming together with the coordinates (l and r) and (x and y) the right-hand coordinate system (l, r, z) and (x, y, z)),
α – angle of attack of the model,
φ – ramp angle.

1. Introduction

One of the interesting specific features of supersonic separated flows is a possibility of existence of extended local regions with gas-dynamic parameters (e.g., total pressure) that differ from the flow parameters in the surrounding flow.

One example of such regions is the region of interaction of shock waves of type IV in Edney's classification [1]. Interaction of the oblique and normal (bow) shock waves C_{01} and C_{02} (Fig. 1, *a*) leads to the formation of a triple

DOI: 10.13009/EUCASS2017-86

configuration of shock waves C_1, C_2 C_T, and the so-called supersonic "jet" *J* in which the total pressure is higher than the total pressure in the subsonic flow surrounding the jet.

The separated flow where such interaction occurs may lead to the formation of a periodic self-sustained flow with pulsations in the frontal separation region (Fig. 2, *a*). This figure shows a sequence of frames composed of instantaneous (with the exposure time of ~ 1 μs) schlieren pictures and illustrating the time evolution of one cycle of pulsations [2]. Each photograph is put into correspondence to a normalized time instant (ranging from 0 to 1), which shows the phase of the process. This flow was first discovered by Mair [3], and the analogy between type IV interaction and the axisymmetric shock wave structure formed in such a case was first noticed by Panaras [4].

The pattern schematically presented in Fig. 1, *b* shows interaction of shock waves in the flow around a blunted body of revolution with a spike, resulting in the formation of a high-total-pressure jet. The supersonic high-total-pressure ring-shaped jet formed due to interaction of the conical C_1 and curved (bow) C_2 shock waves is directed toward the head part of the model (see the pattern in Fig. 2, *b*). The reason for the formation of a periodic self-sustained flow is pumping of the high-pressure gas by the jet into the separated reverse flow region *RF* (time instants 0.4 – 0.68 in the photographs in Fig. 2, *a*), followed by sudden emptying of the separation region due to its radial expansion after the instant when the jet moves away from the body surface (time instants 0.75 – 1.0).

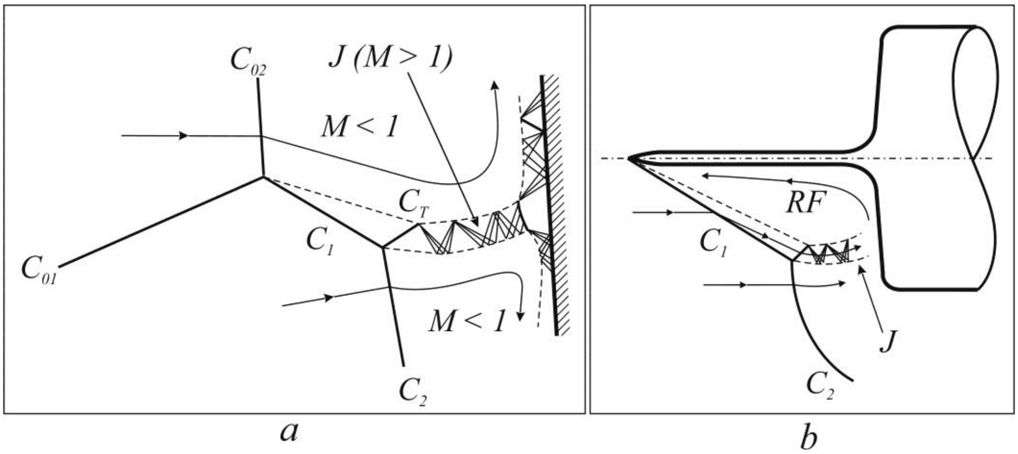

Fig. 1. Interaction of shock waves with the formation of a jet incident onto the model surface: (*a*) type IV interaction (according to [1]); (*b*) axisymmetric analog for a flow with a frontal separation region (according to [4])

Another variant of interaction of shock waves with the formation of a high-total-pressure region of the flow near the wall is illustrated in Fig. 3, *a*. This pattern was presented in [1] on the basis of the data of Deveikis and Sawyer [5, 6]. Interaction of the shock waves C_1 and C_2 leads to the formation of a jet *J* adjacent to the model surface. A known example of such a structure is a hypersonic flow around a double cone considered by Holden et al. (the pattern in Fig. 3, *b* is based on the data of [7]).

According to those results, interaction of the shock wave C_1 attached to the first cone with the shock wave C_3 detached from the second cone leads to the formation of a separation region forming the shock wave C_2. The pattern also shows the reverse flow region *RF* and the slip surface *SS* passing downstream from the line of interaction of the shock waves C_1 and C_2, which separates the gas flow that passed through the shock wave C_2 from the flow that passed through the shock wave C_2'. The shock waves C_2', C_3, and C_T form a triple configuration with an inhomogeneous flow region behind it: supersonic high-total-pressure jet *J* and region of the subsonic low-pressure gas behind the shock wave C_3. Between the model wall and the jet *J*, there is the boundary layer *BL*, where the total pressure is also lower than that in the jet.

It can be noted that the high-pressure region ("jet" *J*) is formed in both cases owing to flow passage through a system of oblique shock waves. The total pressure losses behind the oblique shock waves C_1 and C_T are smaller than that behind the curved shock wave C_2 (or C_3), which is responsible for the difference in the total pressures in the jet *J* and in the flow surrounding the jet. The difference between the above-mentioned situations can be formulated as follows: in the first case, the jet impinges onto the model surface in the close-to-normal direction with respect to the wall; in the second case, the jet moves along the model surface.

Another mechanism of the formation of the high-total-pressure gas region was proposed in [8 – 10]. Based on the results of studying a separated flow in a compression region, it was shown that the high-total-pressure gas region (called the "dynamic layer" by the authors) is formed due to passage of the incoming flow through an expansion fan formed in the flow reattachment region rather than through the shock waves. According to the results obtained, the total pressure in the high-pressure region reached 0.95 of the free-stream total pressure.

DOI: 10.13009/EUCASS2017-86

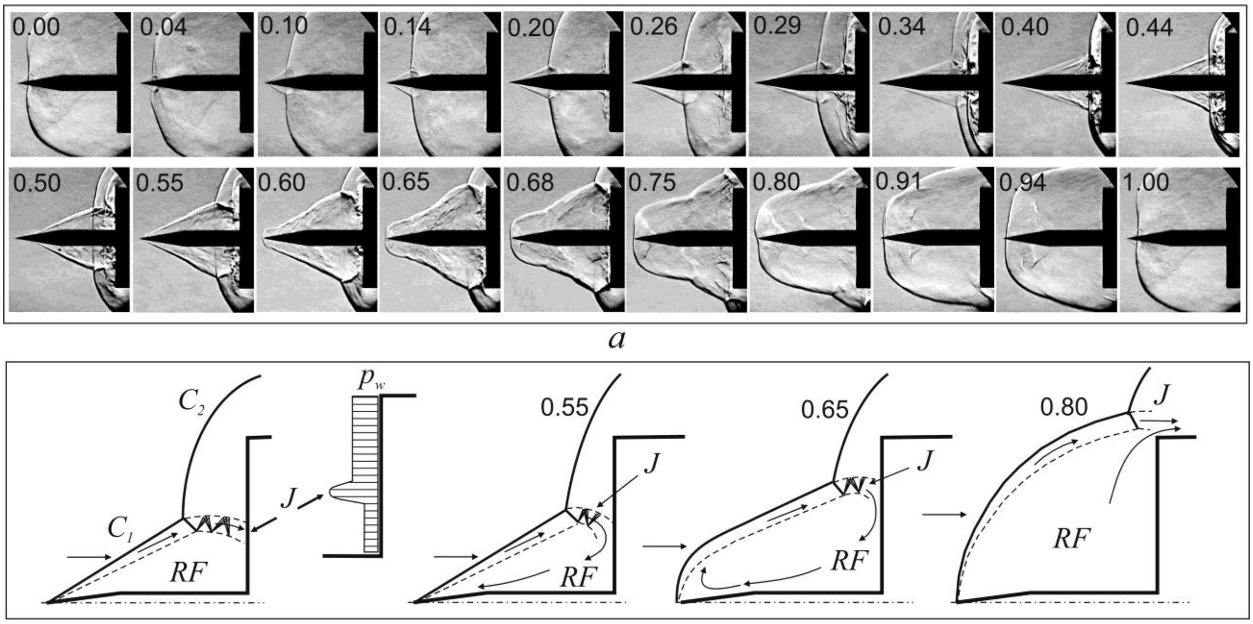

b

Fig. 2. Pulsed flow with the frontal separation region: (a) sequence of photographs of one cycle of pulsations (according to [2]), (*b*) flow pattern with the formation of a high-total-pressure jet *J* in the phase of separation region formation and emptying (according to [4])

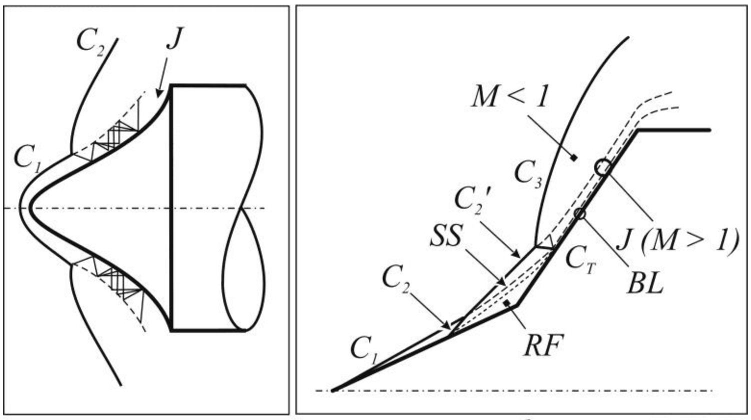

a *b*

Fig. 3. Interaction of shock waves with the formation of a jet adjacent to the model surface: (*a*) flow around a concave body (according to [1] with a reference to [5, 6]); (*b*) flow around a double cone (according to [7])

A schlieren picture of this flow is shown in Fig. 4, *a*, with an explanatory diagram in Fig. 4, *b*. One can see the shock wave C_1 from the leading edge of the compression corner, the separation shock C_2, the reattachment shock C_3, the reverse flow region *RF*, the shear layer *SL* above this region, the zero velocity surface *ZVS*, the reattachment zone *RZ*, the reattachment line *R* (which is normal to the plane of the figure and is shown as a point), the compression fan *CF*, the boundary layer *BL* downstream of the reattachment line, and the high total pressure "dynamic" layer *DL*.

The shear layer *SL* includes four conventional gas flows: 0 – 3 (Fig. 4, *b*). The gas flow indicated by 0 is directly adjacent to the zero velocity surface *ZVS*. The gas in this flow approaches the reattachment line *R*, but does not cross it; instead the gas enters the reverse flow region *RF*. The gas flows denoted by 1, 2, and 3 pass above the reattachment line *R* and are deflected parallel to the ramp wall. A compression fan *CF* is formed in the region ahead of the reattachment pine *R*; at a certain distance from the model wall, this expansion fan transforms to the shock wave C_3. Flow 1 is directly adjacent to the wall and transforms to the boundary layer *BL*. Flow 2 is isentropically turned in the compression fan *CF*. Flow 3 passes through the shock wave C_3. The losses of the total pressure p_0 in layer 1 due to viscosity forces and in layer 3 on the shock wave C_3 are greater than that in the compression fan *CF*, which leads to the formation of the high-total-pressure ("dynamic") layer *DL* above the boundary layer *BL*.

DOI: 10.13009/EUCASS2017-86

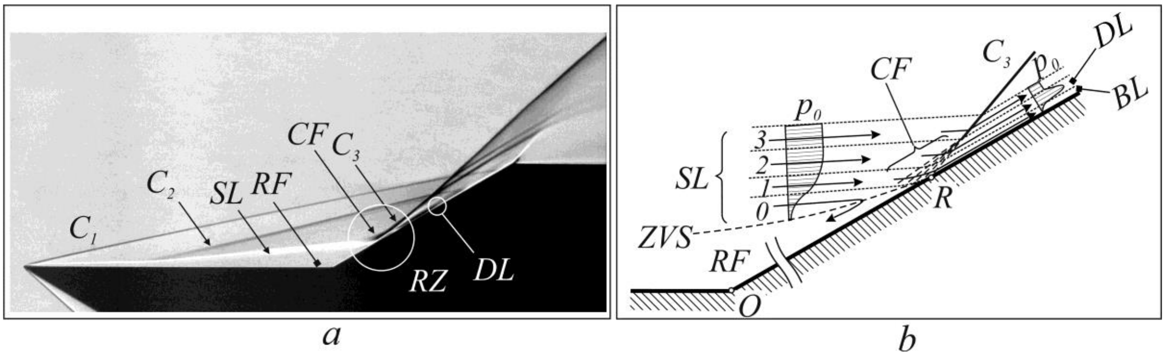

Fig. 4. Supersonic separated flow in a compression corner: (*a*) schlieren picture, (*b*) diagram of the formation of the high-pressure layer *DL* (according to [8, 9])

Only one particular example of such a flow was considered in [8 – 10]: separated flow on a model with a ramp angle $\varphi = 30°$ for the free-stream Mach number $M_\infty = 6$. Therefore, it seems reasonable to study the influence of the model geometry and free-stream Mach number on the characteristics and the region of existence of the high-pressure layer. In the present study, the flow downstream of the reattachment line is considered for the ramp angle varied in the interval $\varphi = 20° – 50°$ in the flow with the Mach number $M_\infty = 6$ or $M_\infty = 8$.

2. Research technique

Four models (Fig. 5, *a*) of the compression corner were studied. All sizes of these models were identical except for the ramp angle, which was varied from 20 to 50 degrees. The length of the horizontal flat plate was $L = 50$ mm. The radius of curvature of the leading edge of the plate was R ~ 5 – 7 μm. The model width was equal to the plate length *L*. The models were made of steel, and the model surfaces were polished.

First a set of models was fabricated, where one plate was equipped with a set of replaceable ramps. These models were used to perform the first test series (series I). After the analysis of results of the first test series, the second set of models (Fig. 5, *a*), which were integrated into one configuration each, was fabricated, and the second test series was performed (series II).

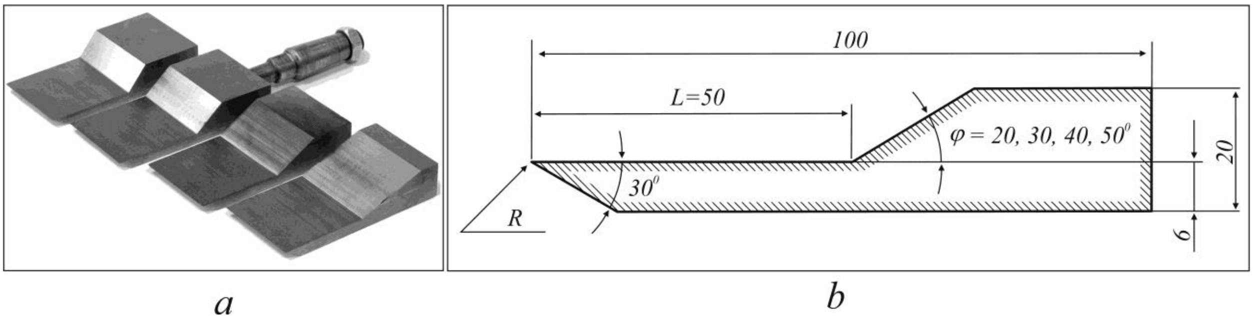

Fig. 5. Model of the compression corner: (*a*) photograph of the models, (*b*) schematic of the model

The experiments were performed in a T-326 hypersonic blowdown wind tunnel based at ITAM SB RAS. The test section is the Eiffel chamber. The wind tunnel is equipped with replaceable contoured axisymmetric nozzles with the exit diameter of 200 mm.

This wind tunnel ensures a homogeneous air flow at a distance $x = 30 – 200$ mm from the nozzle exit, which is shaped as a cylinder 100 mm in diameter. In Fig. 6, the homogeneous flow regions are bounded by black horizontal lines: $50 < y < +50$ mm. For M = 6, the mean Mach number in this region is $M_m = 6.026$, and the mean standard deviation is $M_{Sd} = 0.016$ (0.2 % of the mean value). For M = 8, the mean Mach number in this region is $M_m = 7.985$, and the mean standard deviation is $M_{Sd} = 0.046$ (0.6 % of the mean value). The standard deviation outside this region is slightly higher.

Figure 7 shows the arrangement of the experiment: model mounted in the test section (*a*); the coordinate system for Pitot pressure measurements (*b*) (the Pitot pressure is equal to the total pressure at the measurement point in a subsonic flow and to the total pressure behind the normal shock in a supersonic flow), and the shape of the receiver of the Pitot pressure probe (*c*).

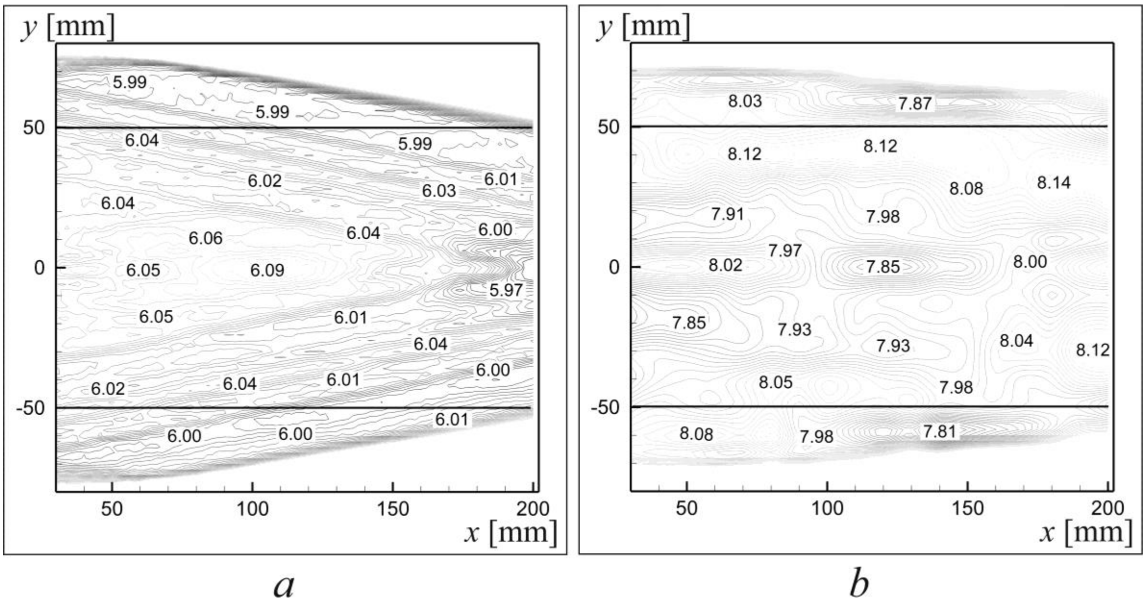

Fig. 6. Mach number field in the test section of the T-326 wind tunnel: (*a*) in the nominal regime with M = 6, (*b*) in the nominal regime with M = 8

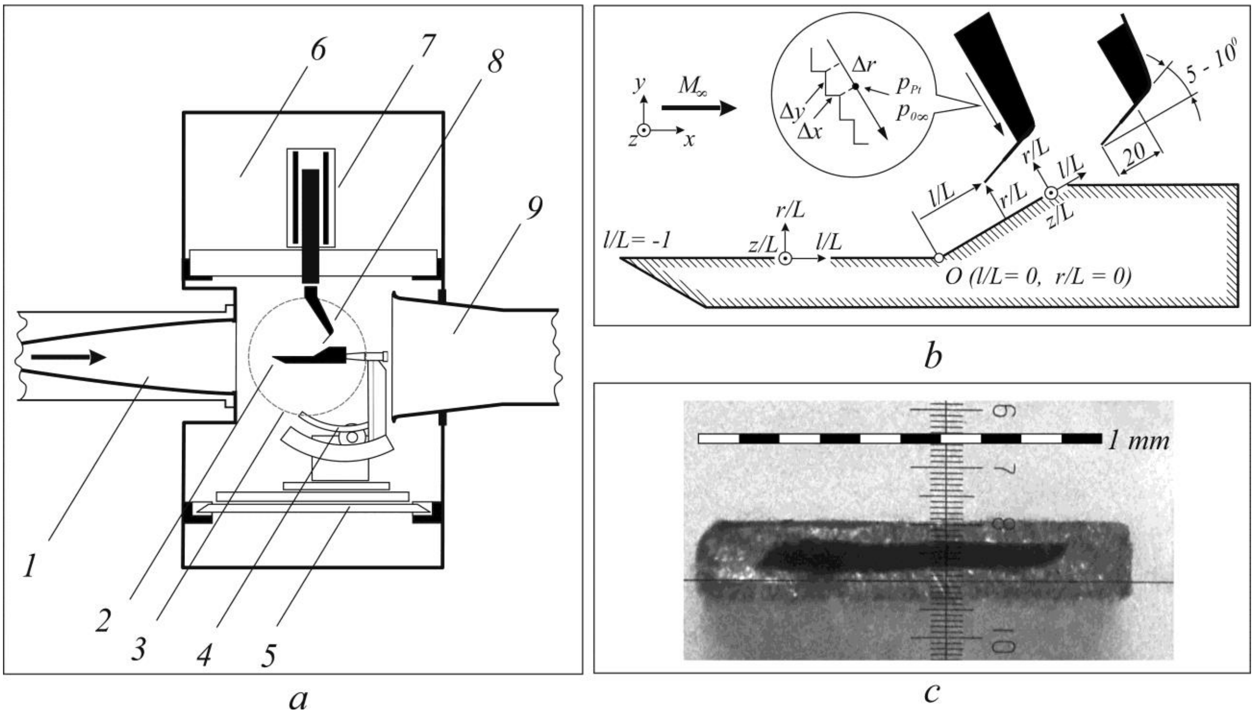

Fig. 7. Arrangement of the experiment: (*a*) model mounted in the wind tunnel; (*b*) measurement of the Pitot pressure above the ramp surface, (*c*) tip of the Pitot probe

The following elements are indicated by numbers in Fig. 7, *a*: 1 – nozzle, 2 – model, 3 – window in the Eiffel chamber for observations, 4 – mechanism for changing the angle of attack of the model (in the present experiment, $\alpha = 0°$), 5 – device for model insertion into the flow, 6 – pressure chamber in the form of the Eiffel chamber, 7 – three-axis traverse system designed for moving the measurement probes, 8 – pylon with the Piror pressure probe, 9 – exhaust diffuser. The wind tunnel is started when the model is yet outside the flow. When a necessary flow regime is reached, the model is inserted into the flow by the device (5) within 1 second. This device is equipped with the so-called alpha-mechanism, which allows the model to be aligned parallel to the incoming flow. The error of model mounting with respect to the free stream is about 0.2°. The model temperature before its insertion into the flow is ~ 295 K.

The main parameters of the experiment are listed in Table 1. The experimental procedure included schlieren visualization of the flow around the model and Pitot pressure measurement above the ramp surface. The visualization was performed by the IAB-451 shadowgraph. The schlieren pictures were obtained with the horizontal

DOI: 10.13009/EUCASS2017-86

position of the Foucault knife, and the exposure time was varied from 3 to 130 μs in different experiments. The photographs were taken by a Videoscan-285/P-USB digital camera. The Pitot pressure was measured by a TDM-A-0.16 probe (the measurement range was $0 – 1.6·10^5$ Pa, and the probe error was smaller than 0.2 % of the measurement range). The pressure probe readings were recorded by an HP Agilent 34970A digital 14-bit multimeter. The pressure in the settling chamber of the wind tunnel was measured by a Metran-150-TAZ probe (the measurement range was $0 – 25·10^5$ Pa, and the measurement error was smaller than 0.1 % of the measurement range). The probe readings were recorded by an IT-8 analog-to-digital module. The maximum deviation from the nominal value (see Table 1) during the experiment was within 0.5%. The temperature in the settling chamber was measured by a chromel-alumel thermocouple, and the signal from the thermocouple was recorded by an ADAM 4018 analog-to-digital module. The error of temperature measurement in the experiment was smaller than one degree. In the course of the experiment, the temperature in the settling chamber could change during the measurement period by 5 – 10 K.

Table 1. Parameters of the experiment in the T-326 hypersonic wind tunnel

Nominal operation mode of the wind tunnel	M = 6	M = 8
Pressure in the settling chamber p_0, Pa	$9.68 \cdot 10^5$	$19.4 \cdot 10^5$
Temperature in the settling chamber T_0, K	390 – 400	620 – 640
Mean Mach number in the homogeneous flow region M_m	6.026	7.985
Reynolds number Re_L	$6.1 \cdot 10^5$	$2.9 \cdot 10^5$
Measurement period, min	5 – 15	

The scheme of measurement of the Pitot pressure profile in the Direction normal to the ramp plane is shown in Fig. 7, *b*. The coordinate system (x, y, z) is fitted to the incoming flow. The origin of the coordinate system is located at the point of intersection of the nozzle axis with the nozzle exit plane. In this coordinate system, commands are given for moving the pylon with the Pitot probe (device 7 in Fig. 7, *a*) by the traverse system; this device allows the probe to be installed with an error smaller than ±20 μm along each of the coordinate axes. The minimum step along each of the coordinates x, y, z is 20 μm.

The coordinate system (l, r, z) is fitted to the model. The origin of this coordinate system (point O) is located in the plane of symmetry on the plane/ramp junction line. The coordinate line l is directed along the model surface, and the line r is normal to the wall. The coordinate z forms the right-hand coordinate system with the lines x, y and l, r. The Pitot pressure profiles measured in the coordinate system (x, y, z) are recalculated to the coordinate system (l, r, z).The coordinate system (l, r, z) is normalized to the plate length L. The measurements were performed in the plane of symmetry of the model (plane z = 0) except for specially mentioned cases.

The pylon with the probe mounted on it is moved to a required cross section l/L at a height r/L above the wall surface. After that, the probe is moved toward the wall at prescribed steps Δx and Δy so that the following relation is satisfied: $(\Delta x^2 + \Delta y^2)^{0.5} = \Delta r$. The pressure was measured at the end of each displacement Δr after a delay necessary for pressure equalization in the measurement pipeline (1 second).

The length of the probe tube is 20 mm. The angle between the tube axis and the model surface (line $O – l$) is 5 – 10 degrees, which is necessary to avoid insertion of disturbances generated by the pylon with the probe into the near-wall flow. The shape of the probe tip is shown in Fig. 7, *c*. The height and width of the probe tip are 0.2 and 1.1 mm, respectively. The height and width of the probe orifice are 0.07 and 0.8 mm, respectively. It is assumed that the probe measures the pressure in the geometric center of the pressure probe tip.

Table 2. Number and coordinates of the measured Pitot pressure profiles

Ramp angle φ, °	20	30	40	50	30
Free-stream Mach number M_∞	6	6	6	6	8
Test series I					
Coordinate of the measurement cross section l/L	0.46; 0.80	0.35	0.38; 0.46	–	0.40
Number of measured Pitot pressure profiles	2; 2	1	1; 1	–	2
Test series II					
Coordinate of the measurement cross section l/L	0.46; 0.70	–	0.38	0.28; 0.32	–
Number of measured Pitot pressure profiles	1; 1 (+1 at z/L = 0.02)	–	2	1; 1	–

When the probe touches the wall, the electrical contact between the probe and model is closed, which is monitored by the probe motion control system. When the contact is closed, the control system issues a signal to

DOI: 10.13009/EUCASS2017-86

terminate probe motion. In this position of the pylon with respect to the wall, it is assumed that the probe coordinate is equal to the half-height of the probe tip above the model surface $r = 0.1$ mm. After that it is possible to calculate the distance r from the wall at which the pressure measurements were performed. This approach allows one to take into account the probe tip displacement with respect to the nominal coordinate (x, y, z) under the action of aerodynamic loads acting on the pylon with the probe. However, this measurement technique does not allow one to control possible premature closure of the electrical contact owing to vibrations of the probe tip under the action of flow pulsations in the near-wall region.

After the coordinate r/L is determined, the Pitot pressure profile $p_{Pt} / p_{0\infty} (r/L)$ is constructed, where the experimentally measured pressure p_{Pt} is normalized to the total pressure measured at the same time in the settling chamber (which is assumed to be equal to the free-stream total pressure $p_{0\infty}$).

Two series of experiments were performed, and 16 Pitot pressure profiles above the ramp wall were measured (see Table 2, where the test series are indicated by Roman numbers I and II).

3. Results

The schlieren pictures of the flow above the compression corner surface are shown in Fig. 8 (one photograph for each examined case except for the case with $\varphi = 50°$, for which two photographs are presented: (1) and (2), which were taken at random time instants). The dashed lines show the cross sections where the Pitot pressure profiles were measured.

The shock wave structures of the flow in all pictures are similar to that in Fig. 4, *a*. The flow structure includes the shock wave generated on the leading edge of the plate, the separation shock, the reattachment shock, the compression fan in the reattachment region, the reverse flow region, and the shear layer above the latter. For the Mach number $M_\infty = 6$, an increase in the ramp angle φ makes the separation line shift upstream over the horizontal plate surface; in the case with $\varphi = 50°$, the separation line closely approaches the leading edge. Moreover, in the case with $\varphi = 50°$, one can see disturbances in the shear layer *SL* above the reverse flow region, which impinge on the reattachment shock C_3; for this reason, the reattachment shock has an inhomogeneous three-dimensional structure and oscillated in space with time.

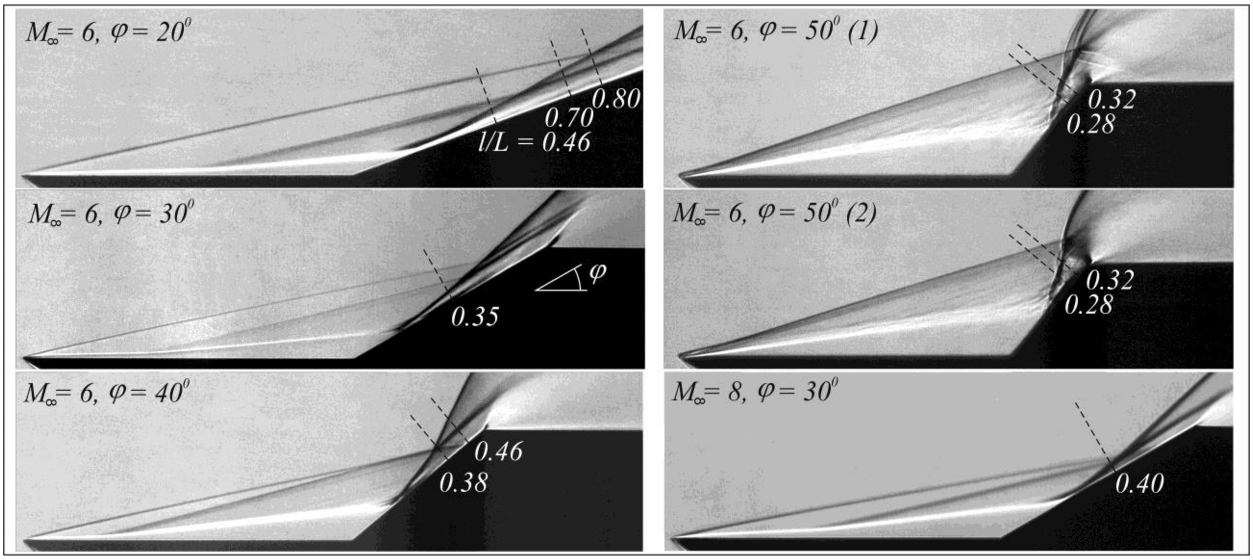

Fig. 8. Schlieren pictures of a supersonic separated flow in a compression corner

To study the flow structure, we compared the schlieren pictures with the pressure measured by the probe. An example of this comparison for the case with $M_\infty = 6$, $\varphi = 20°$, and $l/L = 0.46$ is shown in Fig. 9. Figure 9, *a* shows the schlieren picture of the flow in the region of flow reattachment; one can see the shock waves C_1, C_2, C_3, the compression fan *CF*, and the shear layer *SL* above the reverse flow region. The probe motion is indicated by the dashed line. Figure 9, *b* shows the enlarged fragment of the photograph in Fig. 9, *a*. For convenience of further comparisons, this fragment is turned in the clockwise direction by 20° so that the ramp surface is aligned in the horizontal plane. Typical points of the flow on the Pitot pressure measurement line are indicated by the numbers 1 – 7. In the photograph, the probe is in position 7 and then moves downward until it touches the model wall. The corresponding Pitot pressure profile is shown in Fig. 9, *c*; the vertical coordinate of this profile *r/L* has the same scale as this coordinate in the photograph in Fig. 9, *b*, which allows one to correlate the specific features of the pressure profile with the flow structure in the photograph.

DOI: 10.13009/EUCASS2017-86

The shock waves C_1, C_2, and C_3 are reflected in the pressure profile as points of drastic enhancement of the Pitot pressure if the probe moves from top to bottom (points 6, 5, and 4, respectively). In the supersonic flow region, the Pitot probe measures the total pressure behind the normal shock wave formed by the probe tip. The higher the Mach number ahead of the probe tip, the greater the total pressure loss behind the normal shock and the smaller the Pitot pressure measured by the probe. The greatest loss of the total pressure induced by the shock wave ahead of the probe is observed behind the weak shock C_1, because the Mach number behind this shock has the highest value. For this reason, the Pitot pressure measured behind this shock has the smallest value among all shock waves C_1, C_2, and C_3.

In the domain between the shock C_3 and the model wall, the probe evidences a complex flow (points marked by 3, 2, and 1). When the photographs were taken, the Foucault knife was aligned horizontally, which allows one to observe the vertical gradient of the gas density in the photograph. If we assume that the static pressure behind the shock C_3 is uniformly distributed along the measurement line, then the change in the total pressure in this direction (and, hence, the change in the Pitot pressure) is caused by the change in the dynamic pressure. In turn, the dynamic pressure is directly proportional to the gas density. Therefore, the nonuniformity of the Pitot pressure distribution in the vertical direction is correlated with the nonuniformity of the density distribution. In the photograph in Fig. 9, *b*, the increase in density from top to bottom is shown as dark regions, and the decrease in density is shows by light regions. After the reattachment shock C_3, the density first increases from point 4 to point 3 (dark region), then decreases (points 3 – 2), increases one more time (points 2 – 1), and again decreases near the wall. The same dependence of the Pitot pressure can be seen in Fig. 9, *c*. Therefore, this complicated dependence of the experimentally measured Pitot pressure distribution is confirmed by optical visualization of the flow in the near-wall region.

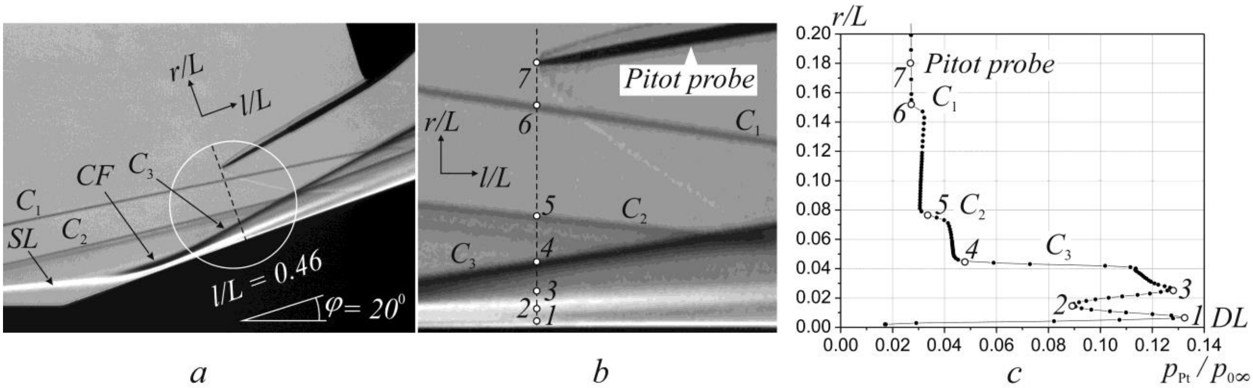

Fig. 9. Correlation between the shock wave structure of the flow with Pitot pressure measurements: (*a*) schlieren picture of the flow, (*b*) magnified fragment of Fig. (*a*) in the region of probe measurements, (*c*) Pitot pressure profile

The profiles of the measured Pitot pressure are shown in Figs. 10 and 11. Figure 10, *a* shows a simplified pattern of the shock wave structure of the flow for $\varphi = 20°$, which includes some elements of the separated flow in the compression corner in the plane of symmetry of the flow. The slip surfaces SS' and SS'' separate the gas flows with different total pressures, which passed through the shock waves C_3, C_3', and C_3''. The test series are indicated by I and II.

The coordinate $r/L = 0$ corresponds to the model wall, and $r/L = 0.002$ is the half-height of the probe tip in the position where it touches the model wall. For $M_\infty = 6$ and $\varphi = 50°$, the lowest position of the probe $r/L = 0$ can be obtained with a small error ($r/L \sim 0.002$) because of premature closure of the electrical contact due to probe tip vibrations under the action of flow pulsations in the near-wall region of the flow.

A local peak of the Pitot pressure (dynamic layer *DL*) is seen in all graphs near the wall at the height $r/L = 0.005 – 0.01$.

Good agreement of the results in the upper part of the Pitot pressure profiles (positions and intensities of the shock waves and slip surfaces) can be noted for different experiments and even different test series (see Fig. 11, *c*, lines 11 and 13). Vice versa, the experimental data in the lower part diverge. The most noticeable differences are observed in the case with $M_\infty = 6$ and $\varphi = 20°$. In Figs. 10, *b* – *d*, one can see regions of reduced Pitot pressure denoted by *LNZ* (local nonuniformity zones).

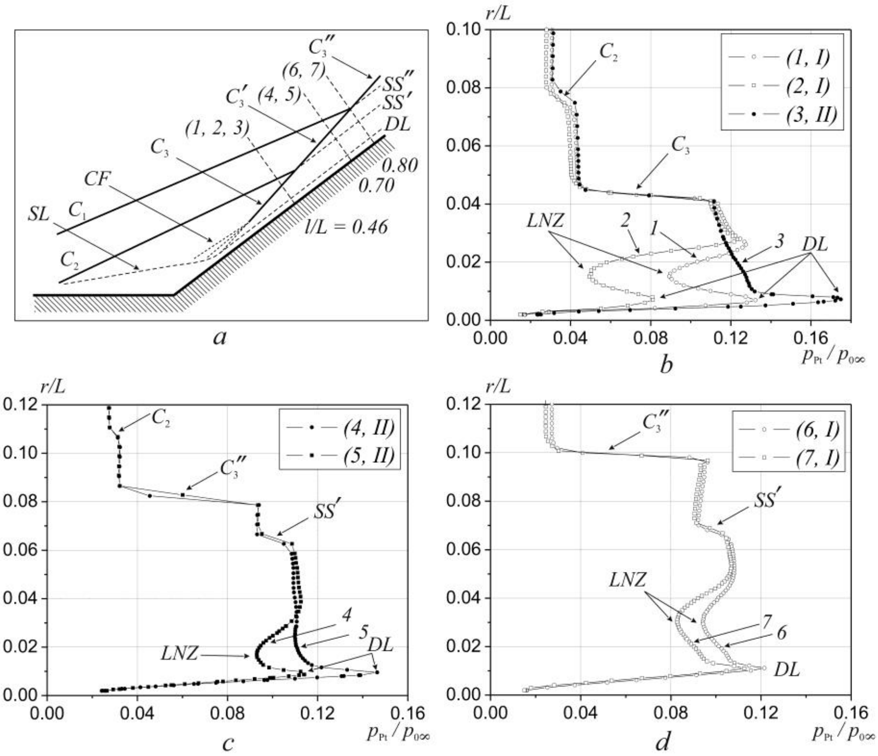

Fig. 10. Flow structure and Pitot pressure distribution near the ramp wall for the case with $M_\infty = 6$ and $\varphi = 20°$: (*a*) simplified pattern of the separated flow in the compression corner, (*b*) Pitot pressure profiles in the cross section *r/L* = 0.47 (curves 1 – 3), (*c*) Pitot pressure profiles in the cross section *r/L* = 0.70 (curves 4 and 5), (*d*) Pitot pressure profiles in the cross section *r/L* = 0.80 (curves 6 and 7)

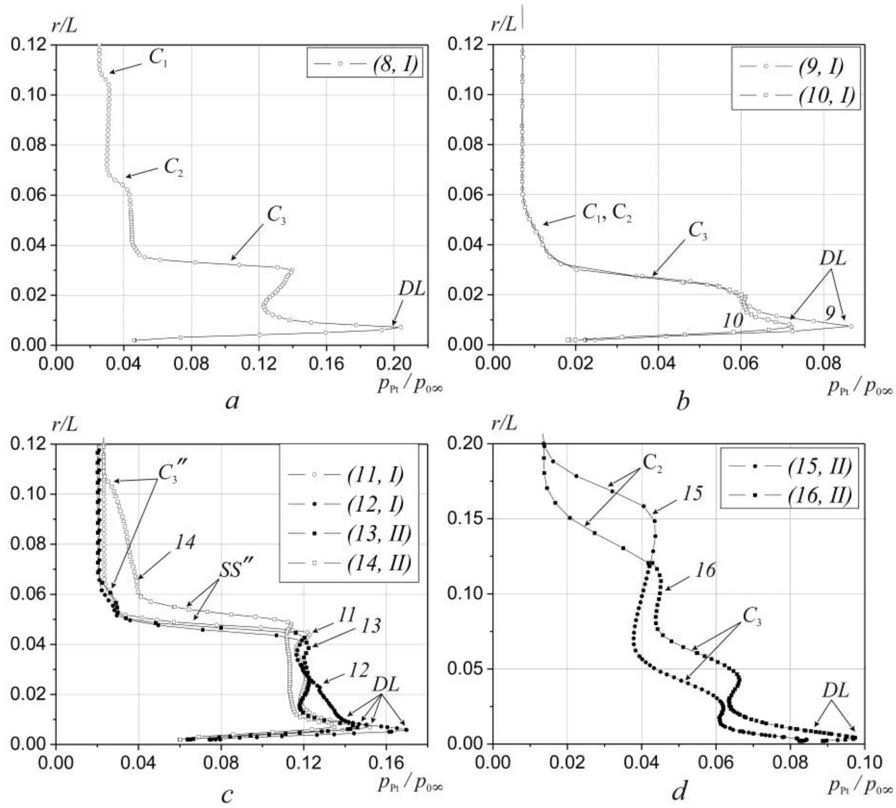

Fig. 11. Pitot pressure distribution near the ramp wall: (*a*) $M_\infty = 6$, $\varphi = 30°$, cross section *r/L* = 0.35 (curve 8), (*b*) $M_\infty = 8$, $\varphi = 30°$, cross section *r/L* = 0.40 (curves 9 and 10), (*c*) $M_\infty = 6$, $\varphi = 40°$, cross sections *r/L* = 0.38 (curves 11, 12, and 13) and *r/L* = 0.46 (curve 14), (*d*) $M_\infty = 6$, $\varphi = 50°$, cross sections *r/L* = 0.28 (curve 15) and *r/L* = 0.32 (curve 16)

These regions are localized not only in the direction of the axis *r*, but also in the transverse direction *z*. In test series II for the case with $M_\infty = 6$, $\varphi = 40°$, and $r/L = 0.70$, we consecutively measured two profile in one experiment, at $z/L = 0$ and $z/L = 0.02$ (curves 12 and 13 in Fig. 11, *c*). In profile 13 corresponding to the coordinate $z/L = 0.02$, there is a local zone *LNZ* with a small decrease in the Pitot pressure above the high-pressure layer, whereas this zone is absent in curve 12.

The formation of such regions is apparently induced by instability of the shear layer *SL* ahead of the reattachment line and of the boundary layer *BL* and dynamic layer *DL* behind this line. The incoming flow always contains a certain number of solid microparticles. When they are incident onto the sharp leading edge, they damage the latter. These damages and also the roughness of the leading edge itself give rise to small disturbances of the boundary layer on the plate, which propagate downstream over the shear layer *SL* into the reattachment region. In the reattachment region, the gas entering this shear flow is deflected with a certain radius of curvature and then moves along the ramp surface. The combined action of centrifugal forces and small local disturbances in the flow turning region may lead to deflection of streamlines from their initial directions and to enhancement of disturbances. It was noted [10] streamwise near-wall Ginoux vortices [11] are observed near the wall at $M_\infty = 6$ and $\varphi = 30°$; the formation of these vortices is caused by the Görtler type instability of the flow. Even if the Görtler number in the reattachment region is smaller than the critical value and streamwise vortices are not formed, it may be assumed that these enhanced disturbances in the near-wall region can still be observed in the form of changes in the total pressure (and Pitot pressure), which are visible in Figs. 10 and 11.

4. Conclusions

The present experimental investigation showed that the high-total-pressure layer is formed in the region of reattachment of a hypersonic separated flow in the range of the ramp angles from 20 to 50°. This observation suggests that such a layer can be also detected in other similar separated flows. For the configurations of the compression corner models considered in the present study, the formation of the high-pressure layer is accompanied by the formation of transverse inhomogeneities of the flow in the reattachment region, which are induced by separated shear flow instability. This instability leads to significant nonuniformity of parameters in the near-wall flow.

This work was supported by the Russian Foundation for Basic Research (Grant No. 16-01-00314a).

REFERENCES

[1] Edney B. Anomalous heat transfer and pressure distribution on blunt bodies at hypersonic speeds in the presence of an impinging shock. Aeronautical Research Institute of Sweden. 1968. Report 115. 93 p.

[2] Zapryagaev V. I., Kavun I. N. Experimental study of the reverse flow in the forward separation region in a pulsating flow around a spiked body // Journal of Applied Mechanics and Technical Physics. 2007. Vol. 48, No. 4. Pp. 492 – 500.

[3] Mair W. Experiments on Separated Boundary Layers on Probes in Front of Blunt Nosed Bodies in a Supersonic Air Stream // Philosophy Magazine. 1952. Vol. 43. Pp. 695 – 716.

[4] Panaras A.G. Pulsating flows about Axisymmetric Concave Bodies // AIAA Journal. 1981. Vol. 19, No. 6. Pp. 804 – 806.

[5] Deveikis W.D., Sawyer J.W. Aerodynamic characteristics of tension shell shapes at Mach 3.0. NASA TN D-3633. 1966. 51 p.

[6] Sawyer J.W., Deveikis W.D. Effects of configuration modifications on aerodynamic characteristics of tension shell shapes at Mach 3.0. NASA TN D-4080. 1967. 38 p.

[7] Nompelis I., Candler G.V, Holden M.S. Effect of Vibrational Non-equilibrium on Hypersonic Double-Cone Experiments // AIAA Journal. 2003. Vol.41, No. 11. Pp. 2162 – 2169.

[8] V.I. Zapryagaev, I.N. Kavun, I.I. Lipatov. Supersonic laminar separated flow structure at ramp for free-stream Mach number 6 // Progress in Flight Physics. Vol 5/ [Edited by Ph. Reijasse, D. Knight, M. Ivanov, I. Lipatov], (EUCASS advances in aerospace sciences book series). EDP Sciences, Torus Press, France, 2013. Pp. 349 – 362.

[9] V.I. Zapryagaev, I.N. Kavun, I.I. Lipatov. High-Pressure Layer Generation in a Compression Corner at a Supersonic Flow Velocity // Fluid Dynamics. 2014. Vol. 49, No. 6. Pp. 819–826.

[10] V.I. Zapryagaev, I.N. Kavun. Formation of streamwise vortices behind the line of supersonic separated flowreattachment at a compression corner // TsAGI Science Journal. 2016. Vol. 47 No.3. Pp. 267 – 281.

[11] Ginoux, J. J. Streamwise Vorticies in Reattaching High-Speed Flows: A suggested Approach // AIAA Journal. 1971. Vol. 9, No. 4. Pp. 759 – 760.